Journal of Neuroscience Methods 382 (2022) 109708

Contents lists available at ScienceDirect

Journal of Neuroscience Methods

journal homepage: www.elsevier.com/locate/jneumeth

Effective R_2 relaxation rate, derived from dual-contrast fast-spin-echo MRI, enables detection of hemisphere differences in iron level and dopamine function in Parkinson's disease and healthy individuals

Jierong Luo, Joanna F. Collingwood *

School of Engineering, University of Warwick, Coventry CV4 7AL, United Kingdom

ARTICLE INFO

Keywords:
Magnetic resonance imaging (MRI)
Transverse relaxation
Parkinson's disease
Asymmetry
Brain iron
Dopamine transporter-specific binding ratio (SBR)

ABSTRACT

Background: Clinical estimates of brain iron concentration are achievable with quantitative transverse relaxation rate R_2, via time-consuming multiple spin-echo (SE) sequences. The objective of this study was to investigate whether quantitative iron-sensitive information may be derived from 3.0 T dual-contrast fast-spin-echo (FSE) sequences (typically employed in anatomical non-quantitative evaluations), as a routinely-collected alternative to evaluate iron levels in healthy (HC) and Parkinson's disease (PD) brains.

New method: MRI 3.0 T FSE data from the Parkinson's Progression Markers Initiative (PPMI) (12 PD, 12 age- and gender-matched HC subjects) were cross-sectionally and longitudinally evaluated. A new measure, 'effective R_2', was calculated for bilateral subcortical grey matter (caudate nucleus, putamen, globus pallidus, red nucleus, substantia nigra). Linear regression analysis was performed to correlate 'effective R_2' with models of age-dependent brain iron concentration and striatal dopamine transporter (DaT) receptor binding ratio.

Results: Effective R_2 was strongly correlated with estimated brain iron concentration. In PD, putaminal effective R_2 difference was observed between the hemispheres contra-/ipsi-lateral to the predominantly symptomatic side at onset. This hemispheric difference was correlated with the putaminal DaT binding ratios in PD.

Comparison with existing method(s): Effective R_2, derived from rapid dual-contrast FSE sequences, showed viability as an alternative to R_2 from SE sequences. Linear correlation of effective R_2 with estimated iron concentration was comparable to documented iron-dependent R_2. The effective R_2 correlation coefficient was consistent with theoretical R_2 iron-dependence at 3.0 T.

Conclusions: Effective R_2 has clinical potential as a fast quantitative method, as an alternative to R_2, to aid evaluation of brain iron levels and DaT function.

1. Introduction

Iron is the most abundant transition metal in the body, and its homeostasis is closely regulated to maintain the basic functions of the organism (Ward et al., 2014). As a component of haemoglobin, iron is essential for oxygen transportation. The many processes for which iron is required include the synthesis of adenosine triphosphate and energy generation in cytochromes. In the brain, iron is an essential co-factor in myelin and neurotransmitter biosynthesis, oxidative phosphorylation, and nitric oxide metabolism. Cellular and thereby regional variations in demand for iron lead to region-specific patterns in the concentration and distribution of iron (Haacke et al., 2005; Ramos et al., 2021). The iron concentration in certain regions of the brain is comparatively high with regard to the human body overall, and as the brain develops there is an age-dependency to iron levels with dynamic change over the human life-span. There is an observed trend towards iron accumulation in the brain in normal ageing (Chen et al., 1989; Zecca et al., 2001; Krebs et al., 2014; Ramos et al., 2014; Hallgren and Sourander, 1958). In a landmark work by Hallgren and Sourander (Hallgren and Sourander, 1958), the non-haemin iron from 81 unfixed, post-mortem brains was quantified using the orthophenanthroline method, after iron extraction from homogenised tissue samples treated with acid. The authors reported empirical relationships for age-dependent iron concentrations for 11 brain regions, featuring the most significant non-haemin iron concentration increase from birth to the age of 50–60 yrs (Hallgren and Sourander, 1958). Recent post-mortem studies also demonstrated brain

* Corresponding author.
E-mail address: J.F.Collingwood@warwick.ac.uk (J.F. Collingwood).

https://doi.org/10.1016/j.jneumeth.2022.109708
Received 8 April 2022; Received in revised form 26 August 2022; Accepted 6 September 2022
Available online 8 September 2022

iron levels changing as a function of normal ageing (Chen et al., 1989; Zecca et al., 2001; Krebs et al., 2014; Ramos et al., 2014), using different techniques including inductively coupled plasma spectroscopy and atomic absorption spectroscopy (AAS). Pathological changes of iron content in particular brain regions also have been reported in several neurodegenerative disorders, such as Alzheimer's disease, Parkinson's disease (Dexter et al., 1991; Mann et al., 1994), Huntington's disease, multiple sclerosis, multiple system atrophy, and neurodegeneration with brain iron accumulation (Visanji et al., 2013; Bartzokis et al., 2007; Kwiatkowski et al., 2012; Liman et al., 2012; Morris and Edwardson, 1994; Qian and Shen, 2001; Schipper, 2012).

Increasing interest has drawn researchers to determine how to detect iron levels in living brains, utilising non-invasive and clinically available techniques such as magnetic resonance imaging (MRI). Primarily stored in ferritin, non-haemin brain iron demonstrates superparamagnetism under an applied external magnetic field at normal body temperature (Schenck, 1996), accelerating the relaxation of neighbouring protons (Schenck, 1996; Gossuin et al., 2009; Gossuin et al., 2016). Several quantitative MRI parameters have been reported to provide a measure of brain tissue iron levels, including transverse relaxation rates R_2 (St Pierre et al., 2005; Hardy et al., 2005; Schenck, 1995; Gelman et al., 1999; House et al., 2007) and R_2* (Chavhan et al., 2009; Hankins et al., 2009; Deistung et al., 2013; Wang et al., 2014), R_2' (Gelman et al., 1999; Qin et al., 2011; Ordidge et al., 1994a), field-dependent R_2 increase (FDRI) (Bartzokis et al., 1994a, 1993, 1994b), and most recently, quantitative susceptibility mapping (QSM) (Langkammer et al., 2012). Among these techniques, derived from clinically established spin-echo (SE) and gradient echo (GRE) pulse sequences respectively, R_2 (St Pierre et al., 2005; Hardy et al., 2005; Schenck, 1995; Gelman et al., 1999; House et al., 2007) and R_2* (Chavhan et al., 2009; Hankins et al., 2009; Deistung et al., 2013; Wang et al., 2014) are widely employed. Described by the static dephasing approximation, GRE-derived R_2* is highly sensitive not only to tissue iron level, but also to the microscopic iron distribution (Yablonskiy and Haacke, 1994). On the other hand, elaborate methods such as FDRI (Bartzokis et al., 1994a, 1993, 1994b) and R_2' (Gelman et al., 1999; Qin et al., 2011; Ordidge et al., 1994a) can reliably detect signal changes introduced by the brain iron level, but they require either multiple acquisitions or specifically refined sequences. Emerging in the past decade, the advanced iron-sensitive mapping technique QSM (Langkammer et al., 2012) employs sophisticated post-processing methods to measure iron-induced susceptibility change from GRE phase information, but it is also sensitive to acquisition parameters and processing algorithms. In this context, R_2, which is comparatively unperturbed by heterogeneous cellular iron distribution and acquisition parameters, remains a reliable approach to measure tissue iron via the characteristic relaxation induced by molecular interactions. Although the mechanisms of the iron enhanced R_2 relaxation are not yet fully understood (Gossuin et al., 2000; Hocq et al., 2015), SE-derived R_2 has demonstrated great sensitivity and specificity to liver iron concentration, and is now established as a clinical tool for quantitative iron imaging (St Pierre et al., 2005).

Nevertheless, the long acquisition time of the SE sequence has been the main disadvantage of the conventional R_2 method in clinical settings, which has been a barrier to its adoption in routine neuroimaging. To generate the R_2 map, four to seven echo images are commonly required for data fitting, where the acquisition time for each echo image of the brain is typically 5–10 min. Attempts to overcome this limitation include a dual-echo SE method (Hardy et al., 2005), where the number of echoes required to fit the observed signal to the exponential decay of the apparent transverse relaxation is minimised. This has shown satisfactory results when the echo times (T_E) were selected carefully (Clark et al., 2003; St Pierre et al., 2004). Multi-echo spin-echo (MESE) may be the most common alternative to the SE, using a single scan of ~ 10 min duration to derive R_2 in the clinical setting, by generating multiple echoes within one repetition with a series of radiofrequency (RF) refocussing pulses. A routine clinical MRI sequence, turbo-spin-echo (TSE) (Fellner et al., 1994; Weigel and Hennig, 2006) (also known as fast-spin-echo (FSE) (Jones et al., 1992)), can further accelerate the scan time compared with the MESE sequence, enabling single- or multiple-echo contrast image acquisition in ~ 5 min. Utilising segmented k-space, the contrast in FSE MRI is determined by the effective T_E at which the MR signal fills in the central k-space, generating brain tissue contrast that is comparable to that obtained by SE and MESE. Due to its versatility in generating MRI contrast and its rapid acquisition, FSE has been made widely available as a routine pulse sequence on clinical scanners from different vendors (Siemens, Philips, GE healthcare), and large datasets have been established through clinical practice and cohort studies (Jack et al., 2008; I. Parkinson Progression Marker, 2011). However, despite the clinical advantages, FSE has not been commonly employed for quantitative assessment because of its rather complex signal formation, and the extent to which there is a quantitative association between FSE-derived MRI measurements and brain iron levels remains to be elucidated.

At clinical field strengths, FSE MRI has been used almost exclusively for anatomical purposes to date, and the sensitivity of the whole brain quantitative FSE-derived transverse relaxation time ($T_2 = 1/R_2$) was reported to be insufficient for diagnostic purposes at 1.5 T (Bauer et al., 2010). Recent efforts were made to recover the 'true' T_2 from the MR images obtained by the FSE sequence by modelling the signal decay (McPhee and Wilman, 2015, 2017; Uddin et al., 2017). However, accurate results require extensive details of acquisition parameters, including the shape of the RF pulse and the actual flip angle, but this information is often unavailable for retrospectively-accessed datasets.

In this study we propose an alternative and straightforward method to utilise dual-contrast FSE data, an attempt to derive a quantitative MRI measure, which we term 'effective R_2', to provide sensitivity to iron levels in the brain. Human brain 3.0 T MRI data available from the Parkinson's Progression Markers Initiative (PPMI), collected from Parkinson's disease patients and healthy control study participants, was evaluated with reference to prior-published post-mortem measures of regional brain iron concentrations. The extent of the effective R_2 as a quantitative MRI method to indicate dopaminergic functional changes in the brain in PD was also investigated in case-control cross-sectional and longitudinal studies.

2. Methods

2.1. PPMI subjects

All participants were screened by the study core of PPMI before enrolment and satisfied the inclusion and exclusion criteria of the PPMI cohort study. Motor, neuropsychiatric and cognitive clinical assessments were performed by the PPMI clinical core for each subject, including Unified Parkinson's Disease Rating Scale (UPDRS), the University of Pennsylvania Smell Identification Test (UPSIT), and Montreal Cognitive Assessment (MoCA). Neuroimaging scans, including structural MRI and dopamine transporter single-photon emission computerised tomography (SPECT) imaging were performed by the imaging core for each subject at screening.

PPMI inclusion criteria for Parkinson's disease (PD) participants were to: 1) have been diagnosed as having PD for $\leq$ 2 years at screening; 2) be aged 30 years or older at the time of PD diagnosis; 3) be at Hoehn and Yahr Stage I or II at PPMI study baseline (0-month); 4) have had at least two of the following symptoms: resting tremor, bradykinesia, rigidity (must have either resting tremor or bradykinesia) or either asymmetric resting tremor or asymmetric bradykinesia; 5) have had confirmation from the PPMI imaging core that their screening dopamine transporter SPECT scan was consistent with dopamine transporter deficit; 6) not be expected to require PD medicine within 6 months of baseline. The exclusion criteria were: 1) subjects taking PD medication (levodopa, dopamine agonists, MAO-B inhibitors, or amantadine), or having taken PD medication within 60 days, or for more than a total of

60 days, prior to baseline; 2) to have received medicines (neuroleptics, metoclopramide, alpha methyldopa, methylphenidate, reserpine, or amphetamine derivative) that might interfere with dopamine transporter SPECT imaging within 6 months of screening; 3) use of investigational drugs or devices within 60 days of baseline.

PPMI inclusion criteria for healthy control subjects (HC) required that subjects must be 30 years old or above at screening. Exclusion criteria for HC were to have: 1) any current or active clinically significant neurological disorder, or to have previously obtained an MRI scan with evidence of a clinically significant neurological disorder; 2) received medicines that might interfere with dopamine transporter SPECT imaging with 6 months of screening; 3) used investigational drugs or devices within 60 days of baseline; 4) any MoCA score less than or equal to 26; 5) a first degree relative with idiopathic PD.

2.2. Retrospective MR data selection

All retrospective MR data obtained and analysed in this work were screened and selected from the PPMI MRI database for a rigorous case-control analysis, therefore, criteria were applied to minimise the potential bias introduced by the magnetic field strength, vendors, age, and gender. Retrospective clinical 3.0 T MR data were selected to ensure the highest possible image resolution and signal-to-noise ratio, and the images acquired by Siemens TrioTim system [see Section 2.3] were selected for processing and analysis, as this provided the greatest data availability for cross-sectional and longitudinal analysis. To investigate the impact on MRI of age-dependent iron accumulation, subjects aged 40–60 yrs at baseline were selected. Finally, the MRI data from 12 HC (age range 40.6–60.1 yrs, 7 males and 5 females) and 12 age- and gender-matched, early-stage drug-free PD (age range 39.2–60.3 yrs, 7 males and 5 females) were selected, processed, and analysed.

2.3. MR acquisition

The MR data from PPMI had been acquired with a dual-contrast 2D FSE pulse sequence on Siemens TrioTim (syngo MR B15) system, either 'Axial PD-T2 FSE' or 'Axial PD-T2 FSE FS'. The resulting proton density-weighted and T_2-weighted images were acquired using the following acquisition parameters: repetition time (T_R) = 3000 or 3270 ms, echo spacing (ESP) = 11.2 ms, echo train length (ETL) = 14, effective T_E = 11.2 and 101 ms, flip angle (FA) = 150°, acquisition plane = axial, field of view (FOV) = 256 × 228 mm, matrix size = 256 × 228, in-plane resolution = 1 × 1 mm^2, bandwidth (BW) = 47.6 kHz, percent phase FOV = 0.9, slice thickness = 3 mm, number of slices = 52 or 54.

2.4. DaTScan acquisition and calculation of Striatal Binding Ratio (SBR)

As documented in the PPMI imaging and analysis protocols, functional SPECT imaging of striatal dopamine transporters (DaTScan) was performed for the participants after ^{123}I-ioflupane injection. The SPECT data were reconstructed and processed prior to the SBR calculation by the PPMI imaging core. The SBR used in this work is provided by the PPMI study documentation, which was calculated as the uptake density of [regions of interest (ROI) / the occipital cortex (reference tissue)] – 1.

In the PPMI study, the SBR was calculated for the bilateral caudate and putamen, indicating the dopamine receptor associated with dopamine transporter (DaT) uptake in the brain regions.

2.5. Calculation of the effective transverse relaxation rate R_2

Compared with the SE- or MESE-derived R_2, the 'effective R_2' presented here is calculated using the proton density-weighted and T_2-weighted images acquired by the dual-contrast FSE sequence, sampled from the apparent T_2 decay of the signal (Fig. 1).

In an FSE pulse sequence, the noise-free signal is determined by the T_E located at the central k-space, effective T_E ($T_{E(eff)}$) which may be approximated as:

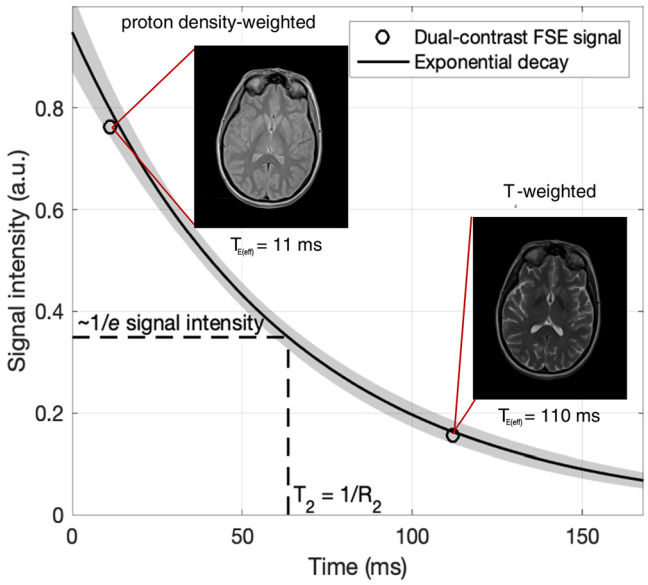

Fig. 1. MR signal decay in the dual-contrast fast-spin-echo (FSE) pulse sequence. $T_{E(eff)}$: effective echo time.

$$S\left(T_{E(eff)}\right) = S_0 e^{-\frac{T_{E(eff)}}{T_2}} \tag{1}$$

where $S\left(T_{E(eff)}\right)$ is the effective T_E-dependent magnitude MR signal, S_0 the signal intensity at time t = 0, and T_2 denotes the corresponding effective transverse relaxation time (effective T_2) to be estimated.

For a dual-contrast sequence:

$$S_{PD}\left(T_{E(eff1)}\right) = S_0 e^{-\frac{T_{E(eff1)}}{T_2}} \quad \text{and} \quad S_{T2}\left(T_{E(eff2)}\right) = S_0 e^{-\frac{T_{E(eff2)}}{T_2}} \tag{2}$$

for the proton density-weighted MR signal and the T_2-weighted signal respectively, as demonstrated in Fig. 1. Hence, the effective R_2 is calculated by the reciprocal of the effective T_2:

$$Effective \quad R_2 = \frac{\ln\left(\frac{S_{PD}}{S_{T2}}\right)}{\Delta T_{E(eff)}} \tag{3}$$

where:

$$\Delta T_{E(eff)} = T_{E(eff2)} - T_{E(eff1)}. \tag{4}$$

Given the high sensitivity of the logarithm to the background noise, the background noise is subtracted from all MR magnitude signals to obtain a zero-mean background before fitting.

2.6. Segmentation

The brain regions known to be particularly rich in iron were manually segmented and measured using ImageJ (Fig. 2), based on a published human brain atlas (Naidich et al., 2009), including bilateral caudate nucleus head (CN), globus pallidus (GP), putamen (PUT), red nucleus (RN) and substantia nigra (SN). The manual segmentation was carried out on consecutive slices of the proton density- and T_2-weighted images to obtain volume measurements of the regions. For repeated longitudinal measurements, a set of ROIs for the individual was segmented based on the baseline acquisition, and this ROI was translated to the follow-up scans, and manually refined where necessary.

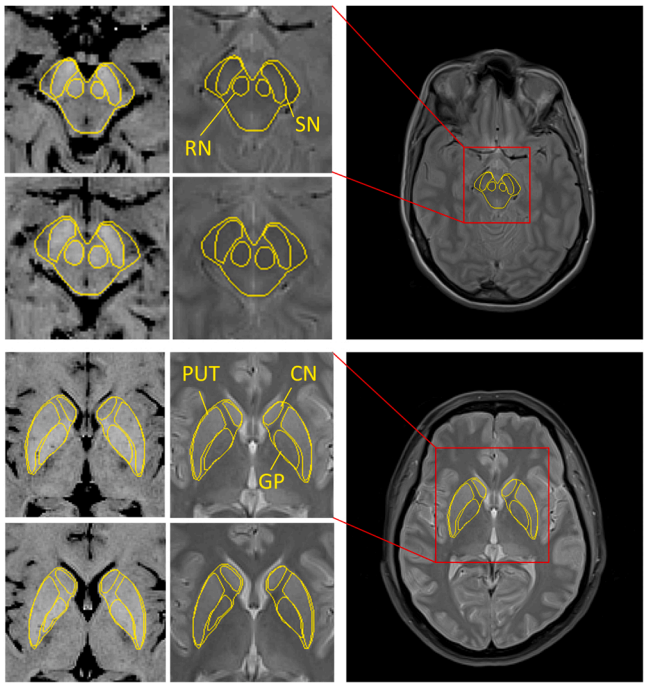

Fig. 2. Example segmentation of in vivo human brain MRI obtained from PPMI. ROI overlay on the effective R_2 parametric maps (left column) derived from effective echo time ($T_{E(eff)}$)= 11 and 101 ms. CN: caudate nucleus, GP: globus pallidus, PUT: putamen, RN: red nucleus, SN: substantia nigra.

2.7. Estimation of brain iron concentration

The average iron concentrations for various brain regions have been reviewed elsewhere (Haacke et al., 2005; Ramos et al., 2021). Although variations in absolute brain iron concentrations have been reported, the relative concentrations between brain regions, as reported in multiple sources, are generally found to be consistent. However, the iron concentration in the healthy brain is known to be dynamic as a function of age (Chen et al., 1989; Zecca et al., 2001; Krebs et al., 2014; Ramos et al., 2014; Hallgren and Sourander, 1958). Therefore, in this study the age-dependent iron concentrations for different brain regions were estimated from Hallgren and Sourander's post-mortem study on unfixed tissue (Hallgren and Sourander, 1958), which contains the largest sample size and the widest age-span in the literature to date.

The iron concentrations in caudate nucleus, globus pallidus, and putamen were calculated for these subjects according Hallgren and Sourander's empirically-derived regression equations relating iron level to the age of the subject (Hallgren and Sourander, 1958). However, the high variation in age-dependent iron concentration prevented equivalent relationships being determined for the substantia nigra and red nucleus, so here we were reliant on simply using the average iron concentration in the substantia nigra and red nucleus, measured respectively from 52 and 44 healthy subjects (age range 30–100 yrs), obtained in the same study (Hallgren and Sourander, 1958).

2.8. Data processing and statistical analysis

The mean, median, and standard deviation of each measurement within the bilateral ROIs were extracted, and the histogram of the pixel values were examined and tested for normality using Shapiro–Wilk test. The mean values and the median values of the effective R_2 were compared and the mean effective R_2 values were used for subsequent analysis.

Any difference in the age and clinical assessment results at baseline (0-month) between HC and PD were tested using the independent t-test for the subject selection. Data normality was tested using Shapiro-Wilk test. Any difference in the effective R_2 measurements between left and right hemispheres were tested using the paired two-samples t-test in the HC and PD groups respectively. To investigate the feasibility of differentiating the brain regions with the effective R_2, the baseline (0-month) measurements of the effective R_2 from bilateral brain regions of participants were calculated by averaging the measurement from the left and right hemisphere in each subject, and then combining these results to find the average value by region for each subject group. Then Friedman's two-way analysis of variance (ANOVA) was employed for all 5 brain regions, with diagnostic groups (i.e. HC and PD) as the between-group variable; subsequently the difference of mean effective R_2 values between each two brain regions was tested using the paired two-samples t-test.

For the remaining analysis, the measured effective R_2 from both hemispheres was calculated for the HC group by averaging as described above. However, the bilateral measurements of the PD subjects were grouped by the symptom-associated hemispheres, according to the asymmetrical laterality of the Parkinsonism reported in each individual's PPMI clinical assessment. This is because the unilaterality of motor symptoms and neurodegeneration in PD has been widely observed at onset (Djaldetti et al., 2006; Hobson, 2012; Barrett et al., 2011) and found to affect neuroimaging measurements such as MRI (Wang et al., 2015; Prasad et al., 2018) and SPECT (Sixel-Doring et al., 2011; Booth et al., 2015a, 2015b; Pagano, 12 et al., 2016). Hence, in this study, the lateral effective R_2 measurements from each brain region in the PD patients were then analysed in two hemispheric groups: the hemisphere contralateral to the individual's PD symptom predominance at onset (PD contralateral), and the ipsilateral hemisphere (PD ipsilateral). The disease unilaterality for individual PD patients as referred to in this study was directly and individually assessed by PPMI at the study enrolment, and the laterality was reported as a part of the subject's clinical assessment result.

To investigate the correlation of effective R_2 and brain iron levels, linear regression analysis with the least-squares method was performed between the measured effective R_2 values and the estimated iron concentration based on the subject's age (Hallgren and Sourander, 1958), in HC, PD contralateral and PD ipsilateral groups respectively. As predictive regression models for iron levels in substantia nigra and red nucleus as a function of age are not available from the same report, the published average iron concentrations for these two regions (Hallgren and Sourander, 1958) were used as noted above. A linear model: $effectiveR_2(s^{-1}) = k[Fe](mg/100g\ \text{wet weight}) + C$, was employed for the regression analysis, where k and C denote the slope coefficient and the intercept offset respectively. The individually observed effective R_2 measurements employed for the analysis, are weighted by $\frac{1}{\sigma^2(effectiveR_2)}$, where σ denotes the standard deviation of the pixelwise measurement within the individual ROI on the effective R_2 maps. Regression analysis was also performed to investigate any relationship between the effective R_2 measurement and motor dysfunction (described by the UPDRS Part III score). To investigate the relationship between the effective R_2 and the striatal DaT function, regression analysis was performed for HC and PD respectively between the bilateral effective R_2 and the corresponding SBR of caudate nucleus and putamen, and between the hemispheric differences (left-right) of the effective R_2 and the SBR.

For each brain region, the distribution of the effective R_2 measurements in each group was tested for normality using Lilliefors test. For between-group comparisons, equal variance was tested by the two-sample F-test. The independent-samples Mann-Whitney U test was performed to test for equal medians between the effective R_2 values obtained from HC and each PD hemispheric group. Any difference between the two hemispheres (contralateral vs. ipsilateral) of PD patients was tested for using the related-samples Wilcoxon signed rank test. The null hypothesis was rejected at the 5% significance level ($p < 0.05$) for all hypothesis testing. The analysis was carried out cross-sectionally for

Table 1
Subject information at baseline. HC: healthy control, PD: Parkinson's disease, UPDRS: Unified Parkinson's Disease Rating Scale score, UPSIT: University of Pennsylvania Smell Identification Test score, MoCA: Montreal Cognitive Assessment score, N: number of subjects. *A non-parametric independent-samples Mann-Whitney U test was performed for the MoCA data which had a non-normal distribution.

	HC (N = 12)	PD (N = 12)	*p*
Gender (M/F)	7/5	7/5	n/a
Age (year)	49.48 ± 5.55	49.62 ± 6.10	> 0.5
Hoehn & Yahr year	n/a	1.55 ± 0.52	n/a
Disease duration (month)	n/a	2.82 ± 2.44	n/a
UPDRS Total	1.33 ± 1.41	27.82 ± 9.80	< 0.001
UPSIT Total	35.22 ± 2.54	21.63 ± 9.04	< 0.001
MoCA	28.92 ± 1.08	28.25 ± 2.60	> 0.4 *

the measurements obtained at baseline and at each follow-up visit at 12, 24 and 48 months where data were available (N = 11/12, 5/12, 6/11 for HC/PD at 12, 24, 48 months respectively). For the longitudinal analysis, the unavailable longitudinal data were imputed for visualisation purposes (not for hypothesis testing), to minimise the missing data bias. The correction used longitudinal data from corresponding individuals to estimate the missing values via shape-preserving piecewise cubic spline interpolation. The longitudinal trajectories of the absolute effective R_2 values measured within each brain region for each group were plotted and the absolute effective R_2 values measured between each visit compared. The related-samples Wilcoxon signed rank test was performed between the effective R_2 measurements at each visit for individuals from each group respectively, to detect any longitudinal change in the effective R_2. To demonstrate the time-dependent trend for each brain region, the longitudinal change of the effective R_2 for individual participants was also calculated as a percentage change at the 12, 24 and 48 month follow-up studies, with respect to the individual's baseline measurement (0 months). All statistical analyses were performed within MATLAB (R2019b, MathWorks).

3. Results

3.1. Subject information

The PPMI-acquired MR data in this study were selected to avoid potential bias introduced by differences in vendor and sequence, and the HC and PD subjects were age- and gender-matched. All subjects selected were right-handed. Subject information at baseline and clinical assessment results are summarised in Table 1. The age distribution for the two diagnostic groups showed no significant difference ($p > 0.05$) at baseline. Compared with HC, the early-stage (average Hoehn & Yahr = 1.55 ± 0.52 yrs) PD group showed significant olfactory degeneration (UPSIT, $p < 0.05$), but no cognitive decline (MoCA, $p > 0.4$).

3.2. Effective R_2 in various brain regions at baseline

As no statistically significant effective R_2 difference had been found between the left and right hemispheres of HC or PD ($p > 0.1$, paired two-samples t-test), between-region analysis of effective R_2 at baseline by brain region was performed after averaging the measurement from the left and right hemisphere in each subject, and then combining these results to find the average value by region for each subject group. At baseline, Friedman's two-way ANOVA showed statistically significant differences ($F > 1$, $p < 0.05$) between the effective R_2 of different brain regions. Moreover, in the HC group, the baseline effective R_2 was found to be significantly different between brain regions (paired 2-sample t-test, $p < 0.05$), except for comparisons of the substantia nigra and red nucleus (Table 2). Compared with the prior-published iron concentration difference (Hallgren and Sourander, 1958) between the brain regions, the baseline effective R_2 difference between the substantia nigra and the putamen (SN - PUT) in HC is lower than expected but statistically significant ($p = 0.001$), with a value smaller than for the comparisons between globus pallidus and substantia nigra (GP - SN) and for putamen and caudate nucleus (PUT - CN).

In HC, baseline effective R_2 values for the individual brain regions are concordant with prior-published average iron concentrations measured in healthy brains (Table 3). However, at baseline the overall effective R_2 difference between HC and PD groups does not show statistical significance ($p > 0.1$).

3.3. Correlation of effective R_2 with estimated iron concentration in the brain

Due to the unilateral nature of PD (Djaldetti et al., 2006; Hobson, 2012; Barrett et al., 2011), the effective R_2 measurements were analysed by the hemispheres contralateral and ipsilateral to the side of the body

Table 2
Baseline effective R_2 difference between brain regions compared alongside prior-published brain iron concentration differences by region in healthy controls (HC) (Hallgren and Sourander, 1958). CN: caudate nucleus, GP: globus pallidus, PUT: putamen, RN: red nucleus, SN: substantia nigra, N: number of subjects.

Comparison between brain regions	Published average iron concentration difference in healthy brains (Hallgren and Sourander, 1958)		Observed effective R_2 difference in HC (N = 12)	
	Difference (mg/100 g wet weight)	*p*	Difference (s^{-1})	*P*
GP – SN	2.84	< 0.01	1.61	< 0.001
SN – PUT	5.14	< 0.001	1.43	0.001
PUT – CN	4.04	< 0.001	2.3	< 0.001
SN – RN	n/a	n/a	-0.08	0.72
GP – RN	n/a	n/a	1.53	< 0.001

Table 3
Baseline effective R_2 in healthy control (HC) and Parkinson's disease (PD) subjects in comparison with the prior-published brain iron concentrations (Hallgren and Sourander, 1958). CN: caudate nucleus, GP: globus pallidus, PUT: putamen, RN: red nucleus, SN: substantia nigra, N: number of subjects.

Brain regions	Published average brain iron concentration (mg/100 g wet weight) in healthy brains (Hallgren and Sourander, 1958)	Observed effective R_2 (s^{-1}) at baseline	
		HC (N = 12)	PD (N = 12)
CN	9.28 ± 2.14 (N = 58)	10.48 ± 0.28	10.52 ± 0.56
PUT	13.32 ± 3.43 (N = 56)	12.78 ± 0.65	12.56 ± 0.83
SN	18.46 ± 6.52 (N = 52)	14.21 ± 1.02	14.43 ± 0.91
RN	19.48 ± 6.86 (N = 44)	14.29 ± 0.74	14.04 ± 0.69
GP	21.30 ± 3.49 (N = 55)	15.82 ± 0.81	16.22 ± 0.76

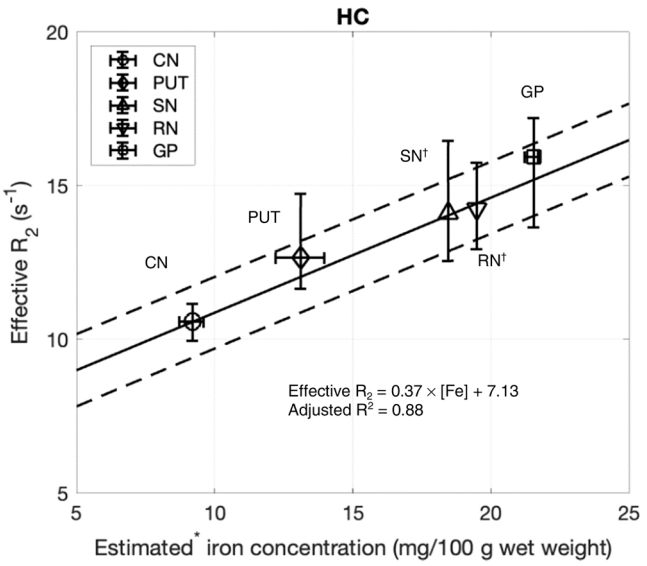

Fig. 3. Linear correlation of the effective R_2 with the estimated iron concentration in healthy controls (HC). Marker: median; error bar: range. †Average iron concentrations are employed. *Estimated from Hallgren & Sourander's study (Hallgren and Sourander, 1958). CN: caudate nucleus, GP: globus pallidus, PUT: putamen, RN: red nucleus, SN: substantia nigra.

where symptoms were predominant at onset. Fig. 3 shows the linear correlation between the iron concentrations estimated as a function of age, from the prior-published post-mortem iron concentration data for healthy brains (Hallgren and Sourander, 1958), and the effective R_2 measurements (n = 175) pooled from all ROIs of healthy individuals for all visits (0/12/24/48 month).

In HC, the results demonstrated a linear correlation (Pearson's $\rho >$ 0.88, F >> 1, $p <<$ 0.001) between the observed effective R_2 and the estimated iron concentration (Fig. 3, Table 4). Compared with the HC group (adjusted $R^2 = 0.88$), less variation of the measured effective R_2 can be explained by the estimated iron concentration in the PD contralateral (adjusted $R^2 = 0.81$) and PD ipsilateral (adjusted $R^2 = 0.81$) groups, whereas the strength of the correlations are comparable ($\rho = 0.8864$, 0.8862 and 0.8699 for HC, PD contralateral and PD ipsilateral, respectively).

Fig. 4 shows individual values of effective R_2 as a function of subject age for HC, PD contralateral and PD ipsilateral, plotted against the age-dependent predicted iron level in normal ageing. In the HC group (Fig. 4, top panel), the trend for the age-dependence of effective R_2 in caudate nucleus, putamen, and globus pallidus was well aligned with the corresponding age-dependent trend in predicted iron concentrations. Larger variations were observed in globus pallidus and putamen of older subjects (age > 54 yrs). In putamen, the effective R_2 also showed a slight overestimation among younger HC (age < 50 yrs). Compared with HC, the effective R_2 demonstrated larger variations in all three brain regions in both contralateral (Fig. 4, middle panel) and ipsilateral (Fig. 4, lower panel) PD hemispheres, compared with the iron levels predicted for normal ageing. The value of effective R_2 was elevated for the globus pallidus in PD, and the effective R_2 in the putamen declined with age in PD contralateral and ipsilateral hemispheres, relative to predicted age-dependent iron levels in HC.

3.4. Comparison of median effective R_2 values between groups

When comparing ipsilateral and contralateral hemispheres, the PD data showed higher effective R_2 values in putamen at baseline, 12-month, and 24-month measurements (each significant at $p < 0.05$), indicative of higher effective R_2 at the 48-month visit ($p < 0.068$) for ipsilateral versus contralateral putamen (Fig. 5). Indication of a higher effective R_2 (ipsilateral vs. contralateral, $p = 0.05$) was found for the global pallidus at 48 months (Fig. 5). The magnitude of the effective R_2 of the substantia nigra was lower for ipsilateral versus contralateral, but did not reach statistical significance ($p < 0.092$ at the 24-month scan). In the red nucleus and the caudate nucleus, equivalent effective R_2 values were observed between the hemispheres (Fig. S1, Supplementary Material).

For the comparison of HC with either PD hemispheric group, a statistically significantly higher effective R_2 was only found in the globus pallidus of the PD ipsilateral group (at 24 months, $p < 0.05$), compared to HC, and this measure was female-dominated due to the lack of HC data at 24 months (N = 5).

3.5. Relationship between effective R_2 and SBR in putamen and caudate

Fig. 6 shows the PPMI-reported bilateral SBR results with the corresponding effective R_2 in HC and PD at baseline. Manifesting as lower SBR, the decreased presynaptic tracer uptake indicated the dysfunction of DaT in putamen and caudate of the PD bilateral hemispheres compared with HC.

As shown in Table S1 (Supplementary Material), the SBR reduction for PD was more prominent in the contralateral than ipsilateral hemisphere to the side of the body with symptomatic predominance at onset. To investigate hemispheric difference, the correlation between the left-right effective R_2 difference and the corresponding left-right DaT SBR difference in putamen and caudate at baseline was tested. As shown in Fig. 7, the result suggests a positive relationship in putamen between the left-right hemispheric difference of the effective R_2 and of the SBR in PD (Pearson's $\rho = 0.524$, $p = 0.08$), with the presence of an outlier (arrowed) from a patient who showed unstable predominant laterality over the 48-month study (PD4, Table S1 in Supplementary Material and accompanying Data_PPMI.xlsx). A Pearson correlation analysis without the outlier confirmed a strong significant positive linear correlation of the hemispheric SBR difference with the effective R_2 difference in PD putamen at baseline (Pearson's $\rho = 0.932$, $p < 0.001$). In HC putamen a positive trend but no statistically significant correlation was found (Pearson's $\rho = 0.315$, $p > 0.1$), and neither PD or HC exhibited a relationship between these variables in the caudate.

In PD, when the measurements from baseline to 48 months were pooled (Fig. S2, Supplementary Material), the positive linear correlations between the putaminal effective R_2 and the DaT SBR, and between their hemispheric differences, were still significant ($p < 0.05$). Compared with baseline, the positive relationships for pooled data were weaker between the putaminal effective R_2 and the DaT SBR (Pearson's $\rho = 0.467$ vs. 0.359), and between their hemispheric differences (Pearson's $\rho = 0.524$ vs. 0.371), as smaller SBR, and smaller SBR hemispheric difference were observed in the later visits. In caudate, the

Table 4
Summary of the regression analysis between effective R_2 values and estimated iron concentration in different groups. n = number of observations (number of scans of subjects × number of regions per subject), RMSE: root-mean-square error, HC: healthy control, PD: Parkinson's disease.

Group	n	Pearson's ρ	Slope (k)	Intercept (C)	Adjusted R^2	RMSE
HC	175	0.8864	0.37 ± 0.01	7.13 ± 0.15	0.88	0.587
PD contralateral	235	0.8821	0.37 ± 0.01	7.22 ± 0.17	0.81	0.739
PD ipsilateral	235	0.8699	0.38 ± 0.01	7.08 ± 0.17	0.81	0.764

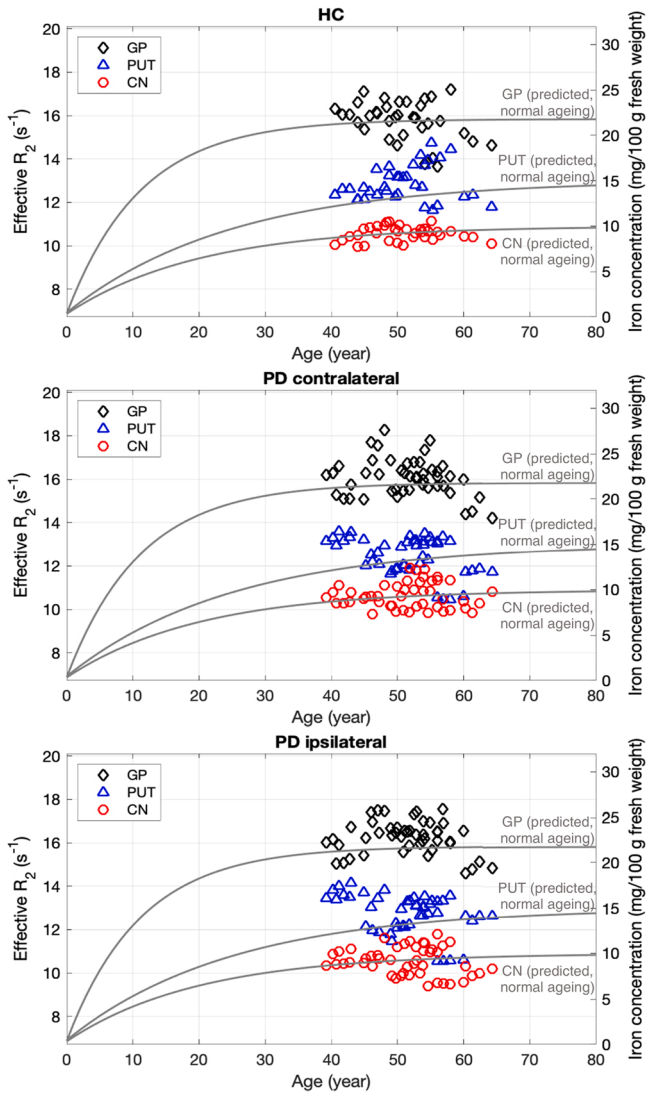

Fig. 4. Observed effective R_2 values for healthy controls (HC), N = 12 (top), and Parkinson's disease (PD), N = 12 contralateral (middle) and ipsilateral (bottom) hemispheres, shown with symbols: diamonds = globus pallidus (GP), triangles = putamen (PUT), circles = caudate nucleus (CN). These effective R_2 values are plotted for visual comparison with prior-published iron concentrations reported for normal ageing (grey lines showing data extracted from Hallgren & Sourander (Hallgren and Sourander, 1958)). The correlation between the two variables: effective R_2 (left y-axis) and iron concentration (right y-axis), was obtained from a weighted linear regression analysis of the observed effective R_2 and the estimated age-dependent iron concentration [Fe] (Hallgren and Sourander, 1958) of the CN, GP, and PUT in HC (n = 105), giving effective $R_2 = (0.42 \pm 0.01) \times [Fe] + (6.73 \pm 0.16)$, adjusted $R^2 = 0.91$, RMSE = 0.534, $F >> 1$, $p << 0.001$. This regression analysis was not extended to the PD observations because the Hallgren & Sourander dataset only evaluated brains from healthy individuals.

corresponding relationships were not statistically significant (Fig. S2, Supplementary Material). Due to the lack of longitudinal SBR results for HC in the PPMI study, the equivalent comparison between HC and PD could not be made in this work.

3.6. Longitudinal change in effective R_2 by brain region

The results provided the longitudinal trajectories of the effective R_2 of individual subjects in different groups (Fig. S3, Supplementary Material), as well as group medians and distributions (Fig. S4, Supplementary Material) after estimation of missing data (see Methods). Up to 48 months, the effective R_2 of PD ipsilateral hemispheres showed an increase in the caudate (12-month to 24-month measurements, $p < 0.05$, Fig. S3, Supplementary Material), but the other longitudinal effective R_2 measures by brain region were largely unchanged from the group median for HC, PD ipsilateral and PD contralateral hemispheres. This was possibly because of the large within-group variation, compared with the subtle longitudinal changes of the effective R_2. Particularly, heterogeneous longitudinal trajectories were observed in caudate nucleus, substantia nigra, and red nucleus in PD ipsilateral and PD contralateral hemispheres, compared with HC subjects. Although no significant longitudinal change was otherwise detected for each group (Fig. S3, Supplementary Material), the most consistent increasing trends were observed in putamen. For all regions, the longitudinal behaviour of effective R_2 did not vary significantly between HC, PD ipsilateral and PD contralateral hemispheres.

To examine normalised longitudinal change at the individual level, the percentage change in effective R_2 with respect to baseline was calculated for each subject (Supplementary Material, Table S2), and the findings are summarised in Fig. S5 (Supplementary Material). The median percentage change of the effective R_2 in HC is small over this 48-month period, when any iron-associated effective R_2 increase with normal ageing for the age-group considered is expected to be near-negligible. In HC, the slight positive increase in effective R_2 after 48 months is consistent with that predicted for caudate nucleus and putamen, but globus pallidus showed a slight decrease.

Substantia nigra was unchanged in HC (−0.2%), whereas small increases in the effective R_2 in PD contralateral and ipsilateral hemispheres were measured (contralateral 1.32% and ipsilateral 1.23% increase from baseline after 48 months). Similarly, a small decrease in red nucleus effective R_2 was observed in HC after 48 months (−1.71%), but not in the contralateral or ipsilateral hemispheres of PD.

The data from these groups did not reveal any statistically significant differences between HC, PD contralateral or ipsilateral hemispheres. It is noteworthy that within-group variation increases over time in all groups, and that heterogeneity in individual longitudinal trajectories persists after minimising baseline variation among subjects.

4. Discussion

4.1. Effective R_2 is linearly proportional to regional brain iron level, offering an alternative to conventional R_2

Based on the results shown in Fig. 5, significantly different effective R_2 values are found for the different brain regions ($p < 0.05$), and the differences correspond to the differentiation of these regions by reported tissue iron concentration (Haacke et al., 2005; Ramos et al., 2021). As shown in Table 3, the baseline effective R_2 values measured in caudate nucleus, putamen, red nucleus, substantia nigra, and globus pallidus are significantly different (except for the comparison of red nucleus with substantia nigra), and a ranking of the magnitude of the effective R_2 values in these brain regions aligns with the predicted corresponding age-dependent iron concentrations from an independent post-mortem study (Hallgren and Sourander, 1958).

When examining the data from HC, evidence that effective R_2 correlates with brain iron concentration is further supported by the regression analysis, with a strong significant linear correlation ($R^2 = 0.88$, $p < 0.05$) for effective R_2 versus estimated brain iron as a function of age (Hallgren and Sourander, 1958). The theoretical iron-dependent coefficient $k_{estimate}$ for conventional R_2 at 3.0 T field strength (B) is as follows (Vymazal et al., 1996):

$$k_{estimate} = 14.1 + 6.2 \times B = 32.7 s^{-1} mg^{-1}/g \approx 0.33 s^{-1} mg^{-1}/100g \quad (5)$$

Here, the slope coefficient found in the present study, $k = 0.37$ s^{-1}/mg/100 g in the HC group is within 12% of this theoretical value.

Compared to conventional R_2 measurement of these brain regions at

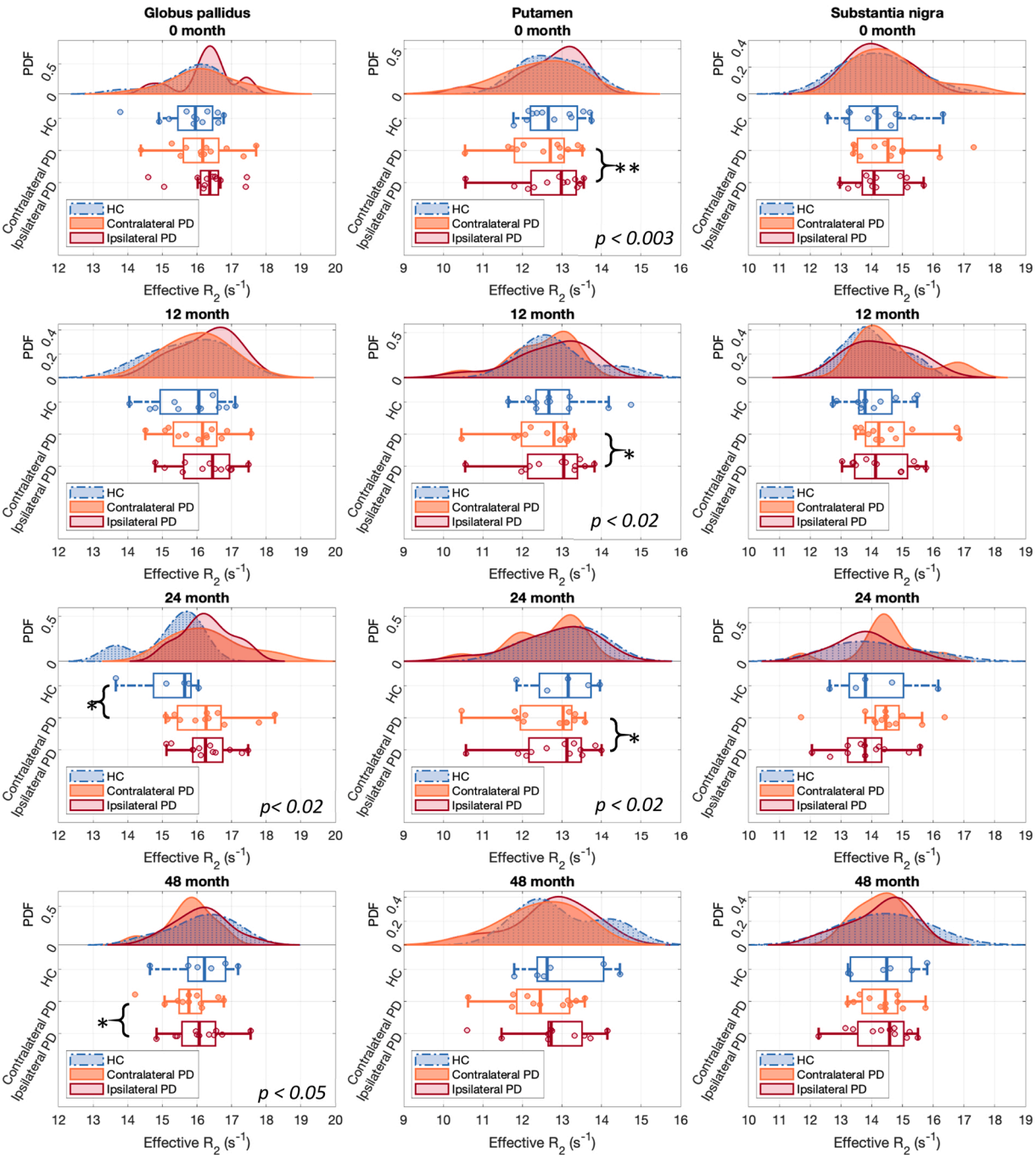

Fig. 5. Effective R_2 measured in globus pallidus (left), putamen (middle), and substantia nigra (right) in healthy controls (HC), Parkinson's disease (PD) contralateral and ipsilateral brain hemispheres at 0, 12, 24, and 48 months. Significant differences indicated as ** ($p < 0.005$), * ($p < 0.05$).

3.0 T (Haacke et al., 2005; Gelman et al., 1999; McPhee and Wilman, 2015; Barbosa et al., 2015), effective R_2 derived from the FSE sequence has a consistently lower magnitude. We suggest that in this case the apparent underestimate may arise from factors including i) the timing of the second effective echo $T_{E(eff)}$ (101 ms), by which point signal from the iron-richer regions of tissue will have largely decayed, and ii) the reduced FA (5/6π) employed in the PPMI dual-contrast FSE sequence, which is common in clinical practice to reduce the specific absorption rate. Nevertheless, although there is a difference in absolute magnitude, the iron-dependent coefficient *k* (slope) for effective R_2 is sufficiently consistent with theoretical predictions that the difference is constrained to being a constant iron-independent offset that will arise from measurement system differences including details of acquisition parameters and pulse sequences.

When examining the data from PD patients, the trends in effective R_2 continue to be consistent with the predicted iron levels (Hallgren and Sourander, 1958), and the correlations found in the current study are in general agreement with reported linear relationships between conventional R_2 and brain iron concentration (Hallgren and Sourander, 1958; Gelman et al., 1999; House et al., 2007; Barbosa et al., 2015; Bartzokis et al., 1994; Drayer et al., 1986). It is concluded that effective R_2 measurements derived from dual-contrast FSE sequences have potential to provide estimates of R_2 in place of the more time-consuming conventional R_2, to indicate brain iron levels.

A key point to consider is whether the linear regression approach is appropriate here, as multiple observations have been made for each

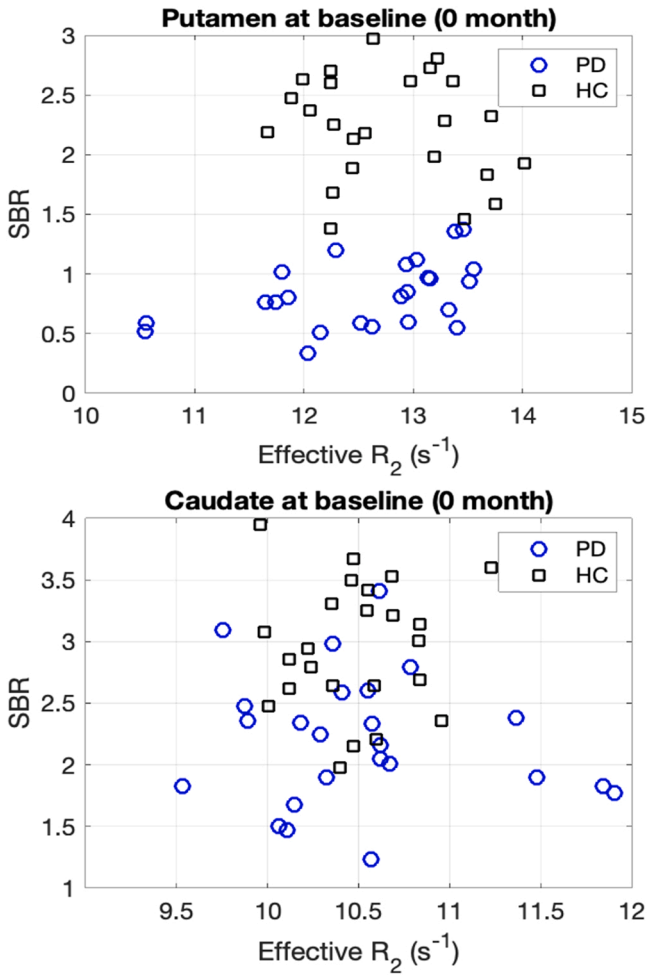

Fig. 6. Bilateral measurements of the effective R_2 and dopamine transporters (DaT) striatal binding ratio (SBR) in the putamen and caudate at baseline.

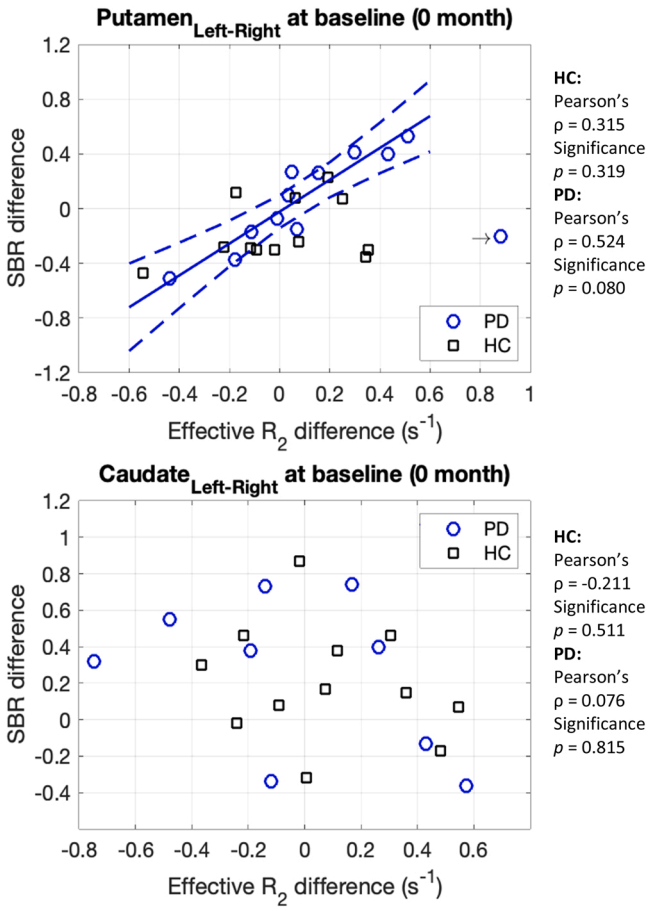

Fig. 7. Correlation between the hemispheric difference of the effective R_2 and dopamine transporters (DaT) striatal binding ratio (SBR) in the putamen and caudate at baseline.

person (multiple regions and multiple time points). The justification arises from the way the independent variable, the estimated iron concentration, was calculated (Method Section 2.7, Page 7), as age is the primary determinant of regional brain iron concentration. In the present work, our use of the empirical relationships established by Hallgren and Sourander (Hallgren and Sourander, 1958) meant that the relationships between the measurements of multiple brain regions from one subject were already modelled by each subject's age. The estimated regional iron concentrations were incremented with age for each individual subject to map to the timeline for the scans they had received as participants in the longitudinal PPMI MRI studies. Therefore, we consider a simpler linear regression analysis suitable for this case, as the known covariant for the observations (age) has been accounted for prior to the fitting. To detect any potential autocorrelation, we also performed residual analysis and tested the residuals with the Durbin-Watson test, and the result showed that the null hypothesis was not rejected ($p > 0.1$), suggesting no first-order autocorrelation. A summary of the linear regression analysis performed for the individual visits for each of the HC and PD groups is included in Supplementary Materials Table S4 and Figs. S6, S7, and S8.

4.2. *Effective R_2 can reveal asymmetric disease manifestation between PD brain hemispheres*

The unilaterality of motor and non-motor symptoms are clinically recognised in PD (Djaldetti et al., 2006; Hobson, 2012; Barrett et al., 2011), and concordant results were found in this work when comparing the group medians of effective R_2 between two PD brain hemispheric groups separated based on asymmetrical disease severity at onset. We showed that in the globus pallidus and putamen, the effective R_2 values were larger in the brain hemisphere ipsilateral to the body side that is predominantly affected by PD at onset, than the contralateral hemisphere (Section 3.4). Conversely, there was no statistically significant hemispheric difference in the substantia nigra in PD brains, which we note is a key region in PD pathogenesis (Damier, 1999). Potential interpretations of these findings include different stages of neurodegeneration in these brain regions, different rates of progression, and domination of the signal attenuation in the dual-contrast FSE images by different mechanisms in the substantia nigra in comparison to the other brain regions evaluated in the PD patients.

The hemispheric differences in the brains of individuals with PD has been previously reported in neuroimaging results, primarily SPECT (Sixel-Doring et al., 2011; Verstappen et al., 2007) and positron emission tomography (PET) (Martin-Bastida et al., 2019; Kumar et al., 2003; Kumakura et al., 2010), and demonstrated as asymmetrically reduced presynaptic striatal tracer uptake by DaT and increased postsynaptic tracer uptake by striatal dopaminergic receptors D_2. Manifested in caudate and putamen, the hemisphere contralateral to the predominantly affected body side showed more severe dysfunction of dopamine transportation, compared with the ipsilateral hemisphere. In substantia nigra, a recent PET study suggested reduced striatal dopamine transporter binding in PD brains, correlated with the pigmentation of the ventral nigra tier in the contralateral hemisphere but not the ipsilateral side (Martin-Bastida et al., 2019). The unilateral reduction of the nigrostriatal terminal density was consistent with the existing

post-mortem observation of asymmetrical neuron loss in the substantia nigra in PD (Kempster et al., 1989). A recent MRI study showed an increase in mean diffusivity and decreased fractional anisotropy in the contralateral putamen, while in the substantia nigra the difference was prominent in the transverse relaxation rates R_2, R_2* and R_2', with larger values observed in the nigra contralateral to the symptomatic body side in 27 PD patients (Wang et al., 2015).

With the effective R_2 derived from the dual-contrast FSE MRI, our results show evidence of these hemispheric differences in PD patients, especially in putamen, with statistically significant differences at baseline, 12 months and 24 months. The hemispheric difference in putamen effective R_2 might be attributed to the asymmetrical reduction of the putaminal dopaminergic fibre density (Kordower et al., 2013), predominant in the contralateral hemisphere, which results in increased diffusivity (Wang et al., 2015) and would account for the decreased effective R_2 reported here. This is further supported by our longitudinal observation of the putamen effective R_2 (Fig. S4, Supplementary Material), where the PD hemispheric difference persists but decreases with time. This is consistent with the prior-reported progressive loss of the dopaminergic fibres in dorsal putamen, where virtually depleted putaminal dopaminergic fibres were observed four years post-diagnosis (Kordower et al., 2013). Hence, the effective R_2 difference between the contralateral and ipsilateral putamen within PD hemispheres becomes marginal over time.

In contrast, more than 50% of the dopaminergic neurons in the substantia nigra have already been lost in the early stages of PD (Damier, 1999; Kordower et al., 2013; Braak et al., 2003), with unilateral depletion (Kempster et al., 1989). Consequently, the impact of previously-documented pathological iron accumulation (Dexter et al., 1991; Sofic et al., 1988; Griffiths et al., 1999; Oakley et al., 2007) on the effective R_2 could be confounded by other pathological changes affecting tissue integrity. Our data are consistent with higher effective R_2 in the PD contralateral hemisphere versus the ipsilateral PD hemisphere and HC, but with great individual and longitudinal variation (Fig. S4, Supplementary Material), especially within the two PD groups where this may arise from asymmetry in changing levels of tissue iron associated with disease pathology, consistent with prior-published MRI observations (Wang et al., 2015). When accounting for effective R_2 signal in the PD substantia nigra, it is important to acknowledge recent biophysical modelling of iron-induced transverse relaxation (Brammerloh et al., 2020; Brammerloh et al., 2021) which attributes the increased transverse relaxation rate in nigrosome 1 predominantly to neuromelanin-bound iron in dopaminergic neurons (rather than iron stored in ferritin). Here, the iron-rich neuromelanin had a significant effect on R_2*, described by the static dephasing approximation (Yablonskiy and Haacke, 1994), whereas for R_2 the signal was considerably affected by nigrosome integrity and was affected to a lesser extent by iron-rich neuromelanin.

4.3. Putaminal effective R_2 in PD corresponds to local DaT dysfunction severity in early-stage PD

The positive linear correlation between the putaminal effective R_2, and the corresponding DaT SBR, suggests that the observed effective R_2 in PD putamen is associated with disease progression as defined by the severity of putaminal DaT dysfunction at baseline (Fig. 6) and during the 48-month period (Fig. S2, Supplementary Material). Moreover, in this study, the results suggest a very strong positive correlation between the effect of putaminal effective R_2 and SBR of stable asymmetrical PD at baseline (Fig. 7). These findings are also consistent with the concept of unilateral progression of putaminal cell loss and dopaminergic fibre density reduction in the PD hemispheres (Kordower et al., 2013), suggesting potential for hemispheric differences in degeneration to be quantified by effective R_2 in early stage PD.

4.4. Effective R_2 measurement of individual brain regions has limited capacity to distinguish HC and PD

Previously reported post-mortem findings using a variety of techniques, including histochemistry, mass spectrometry, AAS, and electron beam microprobe analysis (Dexter et al., 1991; Sofic et al., 1988; Griffiths et al., 1999; Oakley et al., 2007), demonstrated an elevation of iron concentration in dopaminergic neurons within the substantia nigra in brain tissue from individuals with PD compared to HC. This informed our hypothesis that an increased effective R_2 could be observed in PD relative to HC, caused by enhanced proton relaxation induced by elevated accumulation of iron in this brain region.

However, we did not observe evidence of statistically-significant differences in effective R_2 at the level of individual brain regions that would allow PD patients to be distinguished from HC ($p > 0.1$). This might in part be a consequence of the limited sample size, as strict inclusion criteria to match age, gender, vendors and acquisition parameters constrained the number of individuals eligible for inclusion in the analysis. On the other hand, the consistency of the group median data obtained at baseline and at 12 months suggests the observed differences between the study groups are unlikely to be caused by random noise. At baseline and 12 months, the group medians of the effective R_2 values show a rank of PD ipsilateral > PD contralateral > HC in the globus pallidus and in the putamen. In the substantia nigra, the median effective R_2 at baseline, 12 month and 24 months are higher in the PD contralateral hemisphere when compared with the ipsilateral PD hemisphere and with HC.

The effective R_2 values obtained here from substantia nigra in the HC, PD contralateral and PD ipsilateral groups, compare well with prior-reported differences in R_2. An increase in the magnitude of conventional R_2 in the substantia nigra of ~ 4.5% was previously reported for PD compared to HC (Barbosa et al., 2015) using a GRASE sequence at the same field strength (3.0 T), where for HC (N = 30), $R_2 = 20.7 \pm 1.7\ s^{-1}$ and for idiopathic PD patients (N = 20), $R_2 = 21.7 \pm 1.7\ s^{-1}$. Here, at baseline we found an increase of ~ 2.8% in the effective R_2 in the substantia nigra of contralateral PD hemispheres, compared with HC (effective $R_2 = 14.21 \pm 1.06\ s^{-1}$), but not in the ipsilateral PD hemisphere. At 12 months, the PD contralateral and ipsilateral hemispheres showed ~ 4.3% and ~ 2.1% increases respectively in the substantia nigra, in comparison with HC (effective $R_2 = 14.02 \pm 0.9\ s^{-1}$).

The apparent lack of sensitivity of R_2 to changing iron status in the PD substantia nigra may perhaps be explained by signal variations arising from changes to the diffusion coefficient of the tissue, due to neuron loss. This is a common limitation of conventional R_2 – and by extension the concept of an effective R_2 introduced in this work. Neuron death in the substantia nigra manifests at an early stage in PD (Damier, 1999), and can counteract the T_2-shortening effect caused by the iron accumulation (Wang, 9 et al., 2016). In fact, large variations in conventional R_2 among individual PD patients was previously reported by Ordidge et al (Ordidge et al., 1994b). Using a hybrid SE-GRE sequence, Ordidge showed that three out of seven PD patients had abnormal T_2 measurements within the substantia nigra ($T_2 = 123 \pm 82$ ms), and four had similar T_2 values (35.9 ± 4.1 ms) compared to the seven HC (35.1 ± 4.3 ms). Here, our effective R_2 measure derived from an FSE pulse sequence may be also influenced by the water diffusion coefficient changing in relation to neuron death, decreasing the observed effective R_2 (Barbosa et al., 2015). A former study (Georgi et al., 2019) concluded that the effects of microstructural changes on water diffusion and R_2 were negligible in human subcortical grey matter, but their observation was arguably confounded by the fixation of the brain samples (Shatil et al., 2018; Dawe et al., 2009; Birkl et al., 2016). Other studies in the field support our suggestion concerning the altered diffusion properties of the degenerating tissue, including a recent diffusion imaging analysis of the PPMI cohort suggesting cross-sectional and longitudinal increases in non-compartmentalised water ('free water') within the substantia nigra of PD patients (Dzieciol et al., 2021; Ofori et al., 2015, 2015).

Other factors, such as the B_1 effect, long 2nd $T_{E(eff)}$, partial volume effect, and the sample size, may also contribute to the observed variations in signal.

The argument that an increase of the free water in the substantia nigra accounts for these observations is consistent with the asymmetry of findings in the PD ipsilateral and contralateral groups, both for substantia nigra and in comparison with the results from the putamen and globus pallidus. The effective R_2 of the substantia nigra is comparatively lower in the PD ipsilateral group than the contralateral group, whereas the effective R_2 of putamen and globus pallidus is relatively higher in the PD ipsilateral group than the contralateral group. If this is considered in the context of PD progression, the neuron loss in early-stage PD is predominantly in the substantia nigra, with putamen and globus pallidus largely preserved (Halliday et al., 2008; Burke et al., 2008). Therefore, signal attenuation and effective R_2 in the preserved regions might be expected to be dominated by iron concentration in the iron-rich regions, whereas free-water effects are already offsetting iron-associated signal in the substantia nigra. Recent attempts to manually separating the pixels by the dominant contribution (i.e., iron, free water) of the MRI signal by thresholding or modelling (Haacke et al., 2010; Sethi et al., 2018) might provide a future means to account more precisely for the pathology-associated changes in free water.

4.5. Longitudinal change in effective R_2 appears consistent with age-dependent changes in iron levels in HC, and with both iron status and microstructural changes in PD

In line with the previously reported post-mortem observations and MRI results (Hallgren and Sourander, 1958; Langkammer et al., 2012; Thomas et al., 1993; Persson et al., 2015), the longitudinal trend of the effective R_2 in HC reflects iron accumulation with normal ageing in the brain. In the caudate nucleus and the putamen, there is evidence of a slight increase in effective R_2 over the 48-month study period. The absence of an equivalent increasing trend for globus pallidus in this study of subjects aged 40–60 yrs is consistent with effective R_2 paralleling tissue iron status, as non-haemin iron concentration in globus pallidus plateaus at an earlier stage of life (30–40 yrs) (Hallgren and Sourander, 1958).

The value of effective R_2 as a function of time has been examined at the level of the group and of the individual. Within-group variations in absolute effective R_2 for individuals are most pronounced in caudate nucleus, red nucleus, and substantia nigra. A factor contributing to this observation may be partial volume effects (particularly for measures from comparatively small volume regions). However, it might reasonably be assumed that this source of noise would be independent of subject group, and in practice the fluctuation in effective R_2 values as a function of time was more pronounced in PD than HC, especially for the substantia nigra in some individuals over the 48-month study period. The suggestion that this variability in transverse relaxation in PD patients is a genuine disease-associated finding (rather than an artefact of measurement) is supported by observations from two other studies which used R_2 * (Ulla et al., 2013; Wieler et al., 2015). Longitudinal measures of the transverse relaxation rate R_2 * in the substantia nigra showed individual variability in PD patients leading to inconsistent conclusions, where Ulla et al (Ulla et al., 2013). reported longitudinally increased R_2 * values in the substantia nigra of 14 PD patients after 36 months (compared to HC ($N = 18$) showing no statistically-significant change in R_2 *), and in another study no overall change in R_2 * was detected in early-stage PD patients ($N = 19$) after 36 months (Wieler et al., 2015). The authors of these studies suggested that the individual variations in PD substantia nigra R_2 * might be attributed to disease severity as assessed by UPDRS score. In the present study we did not see evidence to support a relationship between UPDRS part III score and effective R_2 in PD substantia nigra ($p > 0.1$).

Although both effective R_2 and R_2* are sensitive to brain iron status, R_2* is obtained with a GRE pulse sequence which is sensitive to field inhomogeneities caused by bulk susceptibility sources in the tissue, such as clustering and locally accumulated iron content. Hence, R_2* is affected by both the concentration and the local distribution of the tissue iron (Kiselev and Novikov, 2018). Therefore, the variation in R_2* from PD substantia nigra might be explained by cellular-level iron status (Oakley et al., 2007; Brammerloh et al., 2020; Zucca et al., 2017; Biesemeier et al., 2016; Lee et al., 2017). By contrast, R_2 and effective R_2 are comparatively insensitive to the microscopic distribution of iron, and can be expected to better reflect the intrinsic molecular and mesoscopic proton relaxation of the biological tissue.

In summary, we demonstrate here a new measure of transverse relaxation that can be derived from a standard rapid clinical sequence: effective R_2, calculated from dual-contrast FSE MRI. Although effective R_2 is necessarily constrained by the sequence design (where with only two echo times there can be no accurate fitting of exponential transverse relaxation behaviours), effective R_2 shows utility as a quantifiable parameter as detailed in this paper and may be widely obtained because dual-contrast FSE is such a widely-employed anatomical MR pulse sequence. Dual-contrast FSE requires much shorter acquisition times than SE or MESE pulse sequences that are used to obtain conventional R_2, and FSE is routinely-used in large-cohort MRI studies available to the research community. As with conventional R_2, the effective R_2 shows evidence of a linear dependence on age-dependent brain iron concentration (Hallgren and Sourander, 1958), with an iron-dependent coefficient comparable to that for conventional R_2 at the same (3.0 T) clinical field strength (Vymazal et al., 1996). Moreover, effective R_2 shows sensitivity to asymmetrical disease progression in PD brain hemispheres. In particular, the effective R_2 of the putamen parallels the hemispherical difference in DaT dysfunction severity in early-stage PD, linearly correlating with hemispherical SBR difference as measured by SPECT. Meanwhile, in healthy controls, the age-dependent longitudinal change in effective R_2 for individual HC are consistent with both confirmed post-mortem and clinical MRI indications of trends in age-dependent brain iron accumulation (Hallgren and Sourander, 1958; Langkammer et al., 2012; Thomas et al., 1993; Persson et al., 2015). Here, the priority was to ensure well-matched datasets, excluding criteria (such as differences in vendor or acquisition sequences) that might affect the values obtained. It would therefore be beneficial to undertake the correlation and longitudinal analyses in larger cohorts in future, when sufficiently large datasets are available, to reduce scope for the influence of variations at the level of the individual.

5. Conclusions

In this work a simple, reproducible method to extract a quantitative measure related to R_2, the 'effective R_2' is demonstrated, calculated from a dual-contrast FSE sequence that is typically used to evaluate anatomy in clinical MRI, and from which the dual echo contrast is normally treated as qualitative. Using MRI data obtained at 3.0 T from participants in the PPMI study, we performed detailed quantitative analysis of the FSE data, evaluating our proposed novel measure of effective R_2 within multiple brain regions in healthy volunteers and individuals with confirmed Parkinson's disease. The cross-sectional and longitudinal analyses in this study indicate that effective R_2 can be a useful quantitative measure obtained from dual-contrast FSE data, exhibiting linear correlation with age-dependent estimates of tissue iron concentration in healthy brains, and showing evidence of sensitivity to measures of Parkinson's disease severity and progression in patients.

Declaration of Competing Interest

The authors declare that they have no known competing financial interests or personal relationships that could have appeared to influence the work reported in this paper.

Data availability

Original data are from the PPMI database, and the measured values from the PPMI MRI scans have been provided as Data_PPMI.xlsx in the online supporting information.

Acknowledgements

This work was supported by a Chancellor's International Scholarship (JL), University of Warwick, Coventry, United Kingdom, and EPSRC grant EP/V007688/1. Data used in the preparation of this article were obtained from the Parkinson's Progression Markers Initiative (PPMI) database (www.ppmi-info.org/data). The data used in this study were from June 2018. For up-to-date information on the PPMI study, visit www.ppmi-info.org. The PPMI study was conducted in accordance with the Declaration of Helsinki and the Good Clinical Practice (GCP) guidelines after approval of the local ethics committees of the participating sites; the PPMI study was approved by the institutional review board of all sites and the radiation safety committee. Written informed consent was obtained from all participants before inclusion in the PPMI study. PPMI – a public-private partnership – is funded by the Michael J. Fox Foundation for Parkinson's Research funding partners 4D Pharma, AbbVie, Acurex Therapeutics, Allergan, Amathus Therapeutics, ASAP, Avid Radiopharmaceuticals, Bial Biotech, Biogen, BioLegend, Bristol-Myers Squibb, Calico, Celgene, Dacapo Brain Science, Denali, The Edmond J. Safra Foundaiton, GE Healthcare, Genentech, GlaxoSmithKline, Golub Capital, Handl Therapeutics, Insitro, Janssen Neuroscience, Lilly, Lundbeck, Merck, Meso Scale Discovery, Neurocrine Biosciences, Pfizer, Piramal, Prevail, Roche, Sanofi Genzyme, Servier, Takeda, Teva, UCB, Verily, and Voyager Therapeutics.

Appendix A. Supporting information

Supplementary data associated with this article can be found in the online version at doi:10.1016/j.jneumeth.2022.109708.

References

Barbosa, J.H., et al., 2015. Quantifying brain iron deposition in patients with Parkinson's disease using quantitative susceptibility mapping, R2 and R2. Magn. Reson Imaging vol. 33 (5), 559–565. https://doi.org/10.1016/j.mri.2015.02.021.

Barrett, M.J., Wylie, S.A., Harrison, M.B., Wooten, G.F., 2011. "Handedness and motor symptom asymmetry in Parkinson's disease,". J. Neurol. Neurosurg. Psychiatry vol. 82 (10), 1122–1124. https://doi.org/10.1136/jnnp.2010.209783.

Bartzokis, G., et al., 1994a. "In vivo evaluation of brain iron in Alzheimer's disease and normal subjects using MRI,". Biol. Psychiatry vol. 35 (7), 480–487.

Bartzokis, G., et al., 1994b. "In vivo MR evaluation of age-related increases in brain iron,". Am. J. Neuroradiol. vol. 15 (6), 1129–1138.

Bartzokis, G., et al., 1994. In vivo MR evaluation of age-related increases in brain iron. AJNR Am. J. Neuroradiol. vol. 15 (6), 1129–1138 ([Online]. Available). ⟨http://www.ncbi.nlm.nih.gov/pubmed/8073983⟩.

Bartzokis, G., et al., 2007. Brain ferritin iron may influence age- and gender-related risks of neurodegeneration. Neurobiol. Aging vol. 28 (3), 414–423. https://doi.org/10.1016/j.neurobiolaging.2006.02.005.

Bartzokis, G., Aravagiri, M., Oldendorf, W.H., Mintz, J., Marder, S.R., 1993. "Field dependent transverse relaxation rate increase may be a specific measure of tissue iron stores,". Magn. Reson. Med. vol. 29 (4), 459–464.

Bauer, C.M., Jara, H., Killiany, R., 2010. "Whole brain quantitative T2 MRI across multiple scanners with dual echo FSE: Applications to AD, MCI, and normal aging☆. NeuroImage vol. 52 (2), 508–514. https://doi.org/10.1016/j.neuroimage.2010.04.255.

Biesemeier, A., et al., 2016. Elemental mapping of Neuromelanin organelles of human Substantia Nigra: correlative ultrastructural and chemical analysis by analytical transmission electron microscopy and nano-secondary ion mass spectrometry. J. Neurochem vol. 138 (2), 339–353. https://doi.org/10.1111/jnc.13648.

Birkl, C., et al., 2016. "Effects of formalin fixation and temperature on MR relaxation times in the human brain,". NMR Biomed. vol. 29 (4), 458–465. https://doi.org/10.1002/nbm.3477.

Booth, T.C., Nathan, M., Waldman, A.D., Quigley, A.M., Schapira, A.H., Buscombe, J., 2015a. "The role of functional dopamine-transporter SPECT imaging in parkinsonian syndromes, part 1,". AJNR Am. J. Neuroradiol. vol. 36 (2), 229–235. https://doi.org/10.3174/ajnr.A3970.

Booth, T.C., Nathan, M., Waldman, A.D., Quigley, A.M., Schapira, A.H., Buscombe, J., 2015b. "The role of functional dopamine-transporter SPECT imaging in parkinsonian syndromes, part 2,". AJNR Am. J. Neuroradiol. vol. 36 (2), 236–244. https://doi.org/10.3174/ajnr.A3971.

Braak, H., Tredici, K.D., Rüb, U., de Vos, R.A.I., Jansen Steur, E.N.H., Braak, E., 2003. "Staging of brain pathology related to sporadic Parkinson's disease,". Neurobiol. Aging vol. 24 (2), 197–211. https://doi.org/10.1016/s0197-4580(02)00065-9.

Brammerloh, M., et al., 2020. "Toward an early diagnostic marker of Parkinson's: measuring iron in dopaminergic neurons with MR relaxometry,". BioRvix. https://doi.org/10.1101/2020.07.01.170563.

Brammerloh, M., et al., 2021. Measuring the iron content of dopaminergic neurons in substantia nigra with MRI relaxometry. Neuroimage vol. 239, 118255. https://doi.org/10.1016/j.neuroimage.2021.118255.

Burke, R.E., Dauer, W.T., Vonsattel, J.P., 2008. "A critical evaluation of the Braak staging scheme for Parkinson's disease,". Ann. Neurol. vol. 64 (5), 485–491. https://doi.org/10.1002/ana.21541.

Chavhan, G.B., Babyn, P.S., Thomas, B., Shroff, M.M., Haacke, E.M., 2009. "Principles, techniques, and applications of T2*-based MR imaging and its special applications,". Radiographics vol. 29 (5), 1433–1449. https://doi.org/10.1148/rg.295095034.

Chen, J.C., et al., 1989. T2 values in the human brain: comparison with quantitative assays of iron and ferritin. Radiology vol. 173 (2), 521–526. https://doi.org/10.1148/radiology.173.2.2798884.

Clark, P.R., Chua-anusorn, W., Pierre, T.G.S., 2003. "Bi-exponential proton transverse relaxation rate (R2) image analysis using RF field intensity-weighted spin density projection: potential for R2 measurement of iron-loaded liver,". Magn. Reson. Imaging vol. 21 (5), 519–530. https://doi.org/10.1016/s0730-725x(03)00080-8.

Damier, P., 1999. The substantia nigra of the human brain: II. Patterns of loss of dopamine-containing neurons in Parkinson's disease. Brain vol. 122 (8), 1437–1448. https://doi.org/10.1093/brain/122.8.1437.

Dawe, R.J., Bennett, D.A., Schneider, J.A., Vasireddi, S.K., Arfanakis, K., 2009. "Postmortem MRI of human brain hemispheres: T2 relaxation times during formaldehyde fixation,". Magn. Reson Med vol. 61 (4), 810–818. https://doi.org/10.1002/mrm.21909.

Deistung, A., Schafer, A., Schweser, F., Biedermann, U., Turner, R., Reichenbach, J.R., 2013. "Toward in vivo histology: a comparison of quantitative susceptibility mapping (QSM) with magnitude-, phase-, and R2*-imaging at ultra-high magnetic field strength,". Neuroimage vol. 65, 299–314. https://doi.org/10.1016/j.neuroimage.2012.09.055.

Dexter, D.T., et al., 1991. Alterations in the levels of iron, ferritin and other trace metals in Parkinson's disease and other neurodegenerative diseases affecting the basal ganglia. no. 4 Brain vol. 114 (Pt 4), 1953–1975. https://doi.org/10.1093/brain/114.4.1953.

Djaldetti, R., Ziv, I., Melamed, E., 2006. "The mystery of motor asymmetry in Parkinson's disease,". Lancet Neurol. vol. 5 (9), 796–802. https://doi.org/10.1016/s1474-4422(06)70549-x.

Drayer, B., Burger, P., Darwin, R., Riederer, S., Herfkens, R., Johnson, G.A., 1986. "MRI of brain iron,". AJR Am. J. Roentgenol. vol. 147 (1), 103–110. https://doi.org/10.2214/ajr.147.1.103.

Dzieciol, K., Iordanishvili, E., Abbas, Z., Nahimi, A., Winterdahl, M., Shah, N.J., 2021. "A robust method for the detection of small changes in relaxation parameters and free water content in the vicinity of the substantia nigra in Parkinson's disease patients,". PLoS One vol. 16 (2), e0247552. https://doi.org/10.1371/journal.pone.0247552.

Fellner, F., et al., 1994. True proton density and T2-weighted turbo spin-echo sequences for routine MRI of the brain. Neuroradiology vol. 36 (8), 591–597 ([Online]. Available). ⟨https://www.ncbi.nlm.nih.gov/pubmed/7862271⟩.

Gelman, N., et al., 1999. "MR imaging of human brain at 3.0 T: preliminary report on transverse relaxation rates and relation to estimated iron content,". Radiology vol. 210 (3), 759–767. https://doi.org/10.1148/radiology.210.3.r99fe41759.

Georgi, J., Metere, R., Jager, C., Morawski, M., Moller, H.E., 2019. "Influence of the extracellular matrix on water mobility in subcortical gray matter,". Magn. Reson Med vol. 81 (2), 1265–1279. https://doi.org/10.1002/mrm.27459.

Gossuin, Y., et al., 2016. NMR relaxation induced by iron oxide particles: testing theoretical models. Nanotechnology vol. 27 (15), 155706. https://doi.org/10.1088/0957-4484/27/15/155706.

Gossuin, Y., Roch, A., Muller, R.N., Gillis, P., 2000. "Relaxation induced by ferritin and ferritin-like magnetic particles: The role of proton exchange,". Magn. Reson. Med. vol. 43 (2), 237–243. https://doi.org/10.1002/(sici)1522-2594(200002)43:2<237::Aid-mrm10>3.0.Co;2-5.

Gossuin, Y., Gillis, P., Hocq, A., Vuong, Q.L., Roch, A., 2009. "Magnetic resonance relaxation properties of superparamagnetic particles,". Wiley Inter. Rev. Nanomed. Nanobiotechnol vol. 1 (3), 299–310. https://doi.org/10.1002/wnan.36.

Griffiths, P.D., Dobson, B.R., Jones, G.R., Clarke, D.T., 1999. "Iron in the basal ganglia in Parkinson's disease,". Brain vol. 122 (4), 667–673. https://doi.org/10.1093/brain/122.4.667.

Haacke, E.M., et al., 2005. Imaging iron stores in the brain using magnetic resonance imaging. " (Eng.), *Magn. Reson Imaging* vol. 23 (1), 1–25. https://doi.org/10.1016/j.mri.2004.10.001.

Haacke, E.M., et al., 2010. Correlation of putative iron content as represented by changes in R2* and phase with age in deep gray matter of healthy adults. J. Magn. Reson Imaging vol. 32 (3), 561–576. https://doi.org/10.1002/jmri.22293.

Hallgren, B., Sourander, P., 1958. "The effect of age on the non-haemin iron in the human brain,". J. Neurochem vol. 3 (1), 41–51 ([Online]. Available). ⟨http://www.ncbi.nlm.nih.gov/pubmed/13611557⟩.

Halliday, G., Hely, M., Reid, W., Morris, J., 2008. "The progression of pathology in longitudinally followed patients with Parkinson's disease,". Acta Neuropathol. vol. 115 (4), 409–415. https://doi.org/10.1007/s00401-008-0344-8.

Hankins, J.S., et al., 2009. R2* magnetic resonance imaging of the liver in patients with iron overload. Blood vol. 113 (20), 4853–4855. https://doi.org/10.1182/blood-2008-12-191643.
Hardy, P.A., Gash, D., Yokel, R., Andersen, A., Ai, Y., Zhang, Z., 2005. "Correlation of R2 with total iron concentration in the brains of rhesus monkeys,". J. Magn. Reson Imaging vol. 21 (2), 118–127. https://doi.org/10.1002/jmri.20244.
Hobson, D.E., 2012. "Asymmetry in parkinsonism, spreading pathogens and the nose,". Park. Relat. Disord. vol. 18 (1), 1–9. https://doi.org/10.1016/j.parkreldis.2011.06.011.
Hocq, A., Luhmer, M., Saussez, S., Louryan, S., Gillis, P., Gossuin, Y., 2015. Effect of magnetic field and iron content on NMR proton relaxation of liver, spleen and brain tissues. Contrast Media Mol. Imaging vol. 10 (2), 144–152. https://doi.org/10.1002/cmmi.1610.
House, M.J., et al., 2007. Correlation of proton transverse relaxation rates (R2) with iron concentrations in postmortem brain tissue from alzheimer's disease patients. Magn. Reson Med vol. 57 (1), 172–180. https://doi.org/10.1002/mrm.21118.
I. Parkinson Progression Marker, 2011. The Parkinson Progression Marker Initiative (PPMI. Prog. Neurobiol. vol. 95 (4), 629–635. https://doi.org/10.1016/j.pneurobio.2011.09.005.
Jack Jr., C.R., et al., 2008. The Alzheimer's Disease Neuroimaging Initiative (ADNI): MRI methods. J. Magn. Reson Imaging vol. 27 (4), 685–691. https://doi.org/10.1002/jmri.21049.
Jones, K.M., et al., 1992. Brain hemorrhage: evaluation with fast spin-echo and conventional dual spin-echo images. Radiology vol. 182 (1), 53–58. https://doi.org/10.1148/radiology.182.1.1727309.
Kempster, P.A., Gibb, W.R., Stern, G.M., Lees, A.J., 1989. "Asymmetry of substantia nigra neuronal loss in Parkinson's disease and its relevance to the mechanism of levodopa related motor fluctuations,". J. Neurol. Neurosurg. Psychiatry vol. 52 (1), 72–76. https://doi.org/10.1136/jnnp.52.1.72.
Kiselev, V.G., Novikov, D.S., 2018. "Transverse NMR relaxation in biological tissues,". Neuroimage vol. 182, 149–168. https://doi.org/10.1016/j.neuroimage.2018.06.002.
Kordower, J.H., et al., 2013. "Disease duration and the integrity of the nigrostriatal system in Parkinson's disease,". Brain vol. 136 (Pt 8), 2419–2431. https://doi.org/10.1093/brain/awt192.
Krebs, N., et al., 2014. Assessment of trace elements in human brain using inductively coupled plasma mass spectrometry. J. Trace Elem. Med Biol. vol. 28 (1), 1–7. https://doi.org/10.1016/j.jtemb.2013.09.006.
Kumakura, Y., et al., 2010. "Elevated [(18)F]FDOPA utilization in the periaqueductal gray and medial nucleus accumbens of patients with early Parkinson's disease,". Neuroimage vol. 49 (4), 2933–2939. https://doi.org/10.1016/j.neuroimage.2009.11.035.
Kumar, A., et al., 2003. [11C]DTBZ-PET correlates of levodopa responses in asymmetric Parkinson's disease. Brain vol. 126 (Pt 12), 2648–2655. https://doi.org/10.1093/brain/awg270.
Kwiatkowski, A., et al., 2012. "Long-term improvement under deferiprone in a case of neurodegeneration with brain iron accumulation,". Park. Relat. Disord. vol. 18 (1), 110–112.
Langkammer, C., et al., 2012. Quantitative susceptibility mapping (QSM) as a means to measure brain iron? A post mortem validation study. Neuroimage vol. 62 (3), 1593–1599. https://doi.org/10.1016/j.neuroimage.2012.05.049.
Lee, H., Baek, S.Y., Chun, S.Y., Lee, J.H., Cho, H., 2017. "Specific visualization of neuromelanin-iron complex and ferric iron in the human post-mortem substantia nigra using MR relaxometry at 7T,". Neuroimage. https://doi.org/10.1016/j.neuroimage.2017.11.035.
Liman, J., Wellmer, A., Rostasy, K., Bahr, M., Kermer, P., 2012. "Transcranial ultrasound in neurodegeneration with brain iron accumulation (NBIA). Eur. J. Paediatr. Neurol. vol. 16 (2), 175–178. https://doi.org/10.1016/j.ejpn.2011.07.009.
Mann, V., et al., 1994. "Complex I, iron, and ferritin in Parkinson's disease substantia nigra,". Ann. Neurol. vol. 36 (6), 876–881.
Martin-Bastida, A., et al., 2019. "Relationship between neuromelanin and dopamine terminals within the Parkinson's nigrostriatal system,". Brain. https://doi.org/10.1093/brain/awz120.
McPhee, K.C., Wilman, A.H., 2017. "Transverse relaxation and flip angle mapping: Evaluation of simultaneous and independent methods using multiple spin echoes,". Magn. Reson Med vol. 77 (5), 2057–2065. https://doi.org/10.1002/mrm.26285.
McPhee, K.C., Wilman, A.H., 2015. "T2 quantification from only proton density and T2-weighted MRI by modelling actual refocusing angles,". Neuroimage vol. 118, 642–650. https://doi.org/10.1016/j.neuroimage.2015.05.079.
Morris, C., Edwardson, J., 1994. "Iron histochemistry of the substantia nigra in Parkinson's disease,". Neurodegeneration vol. 3 (4), 277–282.
Naidich, T.P., Duvernoy, H.M., Delman, B.N., Sorensen, A.G., Kollias, S.S., Haacke, E.M., 2009. Duvernoy's atlas of the human brain stem and cerebellum: high-field MRI, surface anatomy, internal structure, vascularization and 3 D sectional anatomy. Springer Science & Business Media,.
Oakley, A.E., et al., 2007. Individual dopaminergic neurons show raised iron levels in Parkinson disease. Neurology vol. 68 (21), 1820–1825. https://doi.org/10.1212/01.wnl.0000262033.01945.9a.
Ofori, E., et al., 2015. "Longitudinal changes in free-water within the substantia nigra of Parkinson's disease,". Brain vol. 138 (Pt 8), 2322–2331. https://doi.org/10.1093/brain/awv136.
Ofori, E., et al., 2015. Increased free water in the substantia nigra of Parkinson's disease: a single-site and multi-site study. Neurobiol. Aging vol. 36 (2), 1097–1104. https://doi.org/10.1016/j.neurobiolaging.2014.10.029.
Ordidge, R.J., Gorell, J.M., Deniau, J.C., Knight, R.A., Helpern, J.A., 1994a. "Assessment of relative brain iron concentrations using T2–weighted and T2*-weighted MRI at 3 Tesla,". Magn. Reson. Med. vol. 32 (3), 335–341.
Ordidge, R.J., Gorell, J.M., Deniau, J.C., Knight, R.A., Helpern, J.A., 1994b. "Assessment of relative brain iron concentrations usingT2-weighted andT2*-weighted MRI at 3 Tesla,". Magn. Reson. Med. vol. 32 (3), 335–341. https://doi.org/10.1002/mrm.1910320309.
Pagano, G., Ferrara, N., Brooks, D.J., Pavese, N., 2016. "Age at onset and Parkinson disease phenotype,". Neurology vol. 86 (15), 1400–1407. https://doi.org/10.1212/WNL.0000000000002461.
Persson, N., et al., 2015. Age and sex related differences in subcortical brain iron concentrations among healthy adults. Neuroimage vol. 122, 385–398. https://doi.org/10.1016/j.neuroimage.2015.07.050.
Prasad, S., Saini, J., Yadav, R., Pal, P.K., 2018. "Motor asymmetry and neuromelanin imaging: Concordance in Parkinson's disease,". Park. Relat. Disord. vol. 53, 28–32. https://doi.org/10.1016/j.parkreldis.2018.04.022.
Qian, Z.M., Shen, X., 2001. "Brain iron transport and neurodegeneration,". Trends Mol. Med. vol. 7 (3), 103–108.
Qin, Y., et al., 2011. "Investigation on positive correlation of increased brain iron deposition with cognitive impairment in Alzheimer disease by using quantitative MR R2' mapping,". J. Huazhong Univ. Sci. Technol. Med Sci. vol. 31 (4), 578–585. https://doi.org/10.1007/s11596-011-0493-1.
Ramos, P., Santos, A., Pinto, N.R., Mendes, R., Magalhaes, T., Almeida, A., 2014. "Iron levels in the human brain: a post-mortem study of anatomical region differences and age-related changes,". J. Trace Elem. Med Biol. vol. 28 (1), 13–17. https://doi.org/10.1016/j.jtemb.2013.08.001.
Ramos, P., Pinto, E., Santos, A., Almeida, A., 2021. "Reference values for trace element levels in the human brain: A systematic review of the literature,". J. Trace Elem. Med Biol. vol. 66, 126745 https://doi.org/10.1016/j.jtemb.2021.126745.
Schenck, J.F., 1995. "Imaging of brain iron by magnetic resonance: T 2 relaxation at different field strengths,". J. Neurol. Sci. vol. 134, 10–18.
Schenck, J.F., 1996. "The role of magnetic susceptibility in magnetic resonance imaging: MRI magnetic compatibility of the first and second kinds,". Med Phys. vol. 23 (6), 815–850. https://doi.org/10.1118/1.597854.
Schipper, H.M., 2012. Neurodegeneration with brain iron accumulation - clinical syndromes and neuroimaging. Biochim Biophys. Acta vol. 1822 (3), 350–360. https://doi.org/10.1016/j.bbadis.2011.06.016.
Sethi, S.K., et al., 2018. Iron quantification in Parkinson's disease using an age-based threshold on susceptibility maps: The advantage of local versus entire structure iron content measurements. Magn. Reson. Imaging. https://doi.org/10.1016/j.mri.2018.10.001.
Shatil, A.S., Uddin, M.N., Matsuda, K.M., Figley, C.R., 2018. "Quantitative Ex Vivo MRI Changes due to Progressive Formalin Fixation in Whole Human Brain Specimens: Longitudinal Characterization of Diffusion, Relaxometry, and Myelin Water Fraction Measurements at 3T,". Front Med (Lausanne) vol. 5, 31. https://doi.org/10.3389/fmed.2018.00031.
Sixel-Doring, F., Liepe, K., Mollenhauer, B., Trautmann, E., Trenkwalder, C., 2011. "The role of 123I-FP-CIT-SPECT in the differential diagnosis of Parkinson and tremor syndromes: a critical assessment of 125 cases,". J. Neurol. vol. 258 (12), 2147–2154. https://doi.org/10.1007/s00415-011-6076-z.
Sofic, E., et al., 1988. "Increased iron (III) and total iron content in post mortem substantia nigra of parkinsonian brain,". J. Neural Transm. vol. 74 (3), 199–205.
St Pierre, T.G., et al., 2005. Noninvasive measurement and imaging of liver iron concentrations using proton magnetic resonance,". Blood vol. 105 (2), 855–861. https://doi.org/10.1182/blood-2004-01-0177.
St Pierre, T.G., Clark, P.R., Chua-Anusorn, W., 2004. "Single spin-echo proton transverse relaxometry of iron-loaded liver,". NMR Biomed. vol. 17 (7), 446–458. https://doi.org/10.1002/nbm.905.
Thomas, L.O., Boyko, O.B., Anthony, D.C., Burger, P.C., 1993. MR detection of brain iron. AJNR Am. J. Neuroradiol. vol. 14 (5), 1043–1048 ([Online]. Available). ⟨https://www.ncbi.nlm.nih.gov/pubmed/8237678⟩.
Uddin, M.N., McPhee, K.C., Blevins, G., Wilman, A.H., 2017. "Recovery of accurate T2 from historical 1.5 tesla proton density and T2-weighted images: Application to 7-year T2 changes in multiple sclerosis brain,". Magn. Reson Imaging vol. 37, 21–26. https://doi.org/10.1016/j.mri.2016.11.007.
Ulla, M., Bonny, J.M., Ouchchane, L., Rieu, I., Claise, B., Durif, F., 2013. "Is R2* a new MRI biomarker for the progression of Parkinson's disease? A longitudinal follow-up,". PLoS One vol. 8 (3), e57904. https://doi.org/10.1371/journal.pone.0057904.
Verstappen, C.C., Bloem, B.R., Haaxma, C.A., Oyen, W.J., Horstink, M.W., 2007. "Diagnostic value of asymmetric striatal D2 receptor upregulation in Parkinson's disease: an [123I]IBZM and [123I]FP-CIT SPECT study,". Eur. J. Nucl. Med Mol. Imaging vol. 34 (4), 502–507. https://doi.org/10.1007/s00259-006-0258-4.
Visanji, N.P., Collingwood, J.F., Finnegan, M.E., Tandon, A., House, E., Hazrati, L.N., 2013. "Iron deficiency in parkinsonism: region-specific iron dysregulation in Parkinson's disease and multiple system atrophy,". J. Park. Dis. vol. 3 (4), 523–537. https://doi.org/10.3233/JPD-130197.
Vymazal, J., et al., 1996. The relation between brain iron and NMR relaxation times: An invitro study. Magn. Reson. Med. vol. 35 (1), 56–61. https://doi.org/10.1002/mrm.1910350108.
Wang, J., et al., 2015. MRI evaluation of asymmetry of nigrostriatal damage in the early stage of early-onset Parkinson's disease. Park. Relat. Disord. vol. 21 (6), 590–596. https://doi.org/10.1016/j.parkreldis.2015.03.012.
Wang, J.Y., et al., 2016. "Meta-analysis of brain iron levels of Parkinson's disease patients determined by postmortem and MRI measurements,". Sci. Rep. vol. 6, 36669. https://doi.org/10.1038/srep36669.

Wang, Q., Li, K., Quan, Q., Zhang, G., 2014. "R2* and R2 mapping for quantifying recruitment of superparamagnetic iron oxide-tagged endothelial progenitor cells to injured liver: tracking in vitro and in vivo,". Int J. Nanomed. vol. 9, 1815–1822. https://doi.org/10.2147/IJN.S58269.

Ward, R.J., Zucca, F.A., Duyn, J.H., Crichton, R.R., Zecca, L., 2014. "The role of iron in brain ageing and neurodegenerative disorders,". Lancet Neurol. vol. 13 (10), 1045–1060. https://doi.org/10.1016/s1474-4422(14)70117-6.

Weigel, M., Hennig, J., 2006. "Contrast behavior and relaxation effects of conventional and hyperecho-turbo spin echo sequences at 1.5 and 3 T,". Magn. Reson Med vol. 55 (4), 826–835. https://doi.org/10.1002/mrm.20816.

Wieler, M., Gee, M., Martin, W.R., 2015. "Longitudinal midbrain changes in early Parkinson's disease: iron content estimated from R2*/MRI,". Park. Relat. Disord. vol. 21 (3), 179–183. https://doi.org/10.1016/j.parkreldis.2014.11.017.

Yablonskiy, D.A., Haacke, E.M., 1994. "Theory of NMR signal behavior in magnetically inhomogeneous tissues: The static dephasing regime,". Magn. Reson. Med. vol. 32 (6), 749–763. https://doi.org/10.1002/mrm.1910320610.

Zecca, L., et al., 2001. "Iron, neuromelanin and ferritin content in the substantia nigra of normal subjects at different ages: consequences for iron storage and neurodegenerative processes,". J. Neurochem. vol. 76 (6), 1766–1773. https://doi.org/10.1046/j.1471-4159.2001.00186.x.

Zucca, F.A., et al., 2017. Interactions of iron, dopamine and neuromelanin pathways in brain aging and Parkinson's disease. Prog. Neurobiol. vol. 155, 96–119. https://doi.org/10.1016/j.pneurobio.2015.09.012.